Protron-Proton Bremsstrahlung at 204 MeV with a Polarized Beam*

K. W. ROTHE,† P. F. M. KOEHLER,‡ AND E. H. THORNDIKE
Department of Physics and Astronomy, University of Rochester, Rochester, New York,
(Received 12 September 1966; revised manuscript received 2 February 1967)

A proton-proton bremsstrahlung experiment has been completed using 204-MeV, 90% polarized protons incident on a liquid-hydrogen target. The gamma ray was detected in a threshold counter. The two protons were observed in a spark-chamber array giving energy and direction information. Cross sections and gamma ray and proton asymmetries due to the polarized beam were measured. The cross sections obtained agree with the theoretical calculations of Sobel and Cromer, and Duck and Pearce. Ueda's calculation is high by a factor near 2, but properly describes the shape of $(d^2\sigma/d\Omega_\gamma dE_\gamma)$ versus E_γ. Proton asymmetries agree in sign and magnitude with the elastic 210-MeV values. Gamma-ray asymmetries are of the same sign and magnitude as those obtained in our measurements of $p+n\rightarrow d+\gamma$ which agree with photodisintegration calculations. An upper limit of 35 nb has been placed on the production of $p+p\rightarrow p+p^*(p^*\rightarrow p+\gamma)$ decaying to a gamma and a proton for lifetimes $10^{-22}\leqslant\tau\leqslant 10^{-10}$ sec.

I. INTRODUCTION

THE nucleon-nucleon interaction at intermediate energies has been and continues to be the subject of a considerable amount of experimental work. Extensive programs involving the measurement of elastic-scattering cross sections, polarizations, and triple-scattering parameters have been carried out, giving rise to a large body of data.[1] These data have been interpreted in terms of several different theoretical pictures: potentials, both phenomenological[2] and meson-theoretic[3]; boundary-condition models[4]; and dispersion-theoretic calculations.[5] While none can be said to provide a complete understanding of the interaction, there has been convergence towards this goal; often the changes being made (e.g., in the case of phenomenological potentials) are relatively small and, for the most part, can be considered corrections to previous versions. Virtually all of the experimental work gives information on N-N amplitudes with all nucleons *on* the mass shell while at the same time the implications of the pictures transcend this domain and predict the behavior of the interaction *off* the mass shell as well. There is no *a priori* reason to expect that a model which works well on the mass shell should continue properly off the mass shell. On the other hand, in view of the applicability of the models to this latter type of scattering, an adequate description over the entire region should be possible. Beyond this intrinsic interest, the off-shell information is relevant also to few- and many-body calculations of nuclear structure and nuclear matter where the presence of more than two nucleons allows any given pair interaction to be off the mass shell.

The N-N bremsstrahlung reaction $N+N\rightarrow N+N+\gamma$ allows one nucleon to be off the mass shell, roughly by the γ-ray energy, which in the experiment to be described was as large as 95 MeV. This reaction is the most unambiguous source of off-mass-shell information, all others involving more than two strongly interacting particles (e.g., π production or 3 nucleon interactions). Of the three bremsstrahlung reactions: $np\gamma$, $pp\gamma$, $nn\gamma$, the first is expected to have the largest cross section. Vanishing of $E1$ transitions[6] for $pp\gamma$ and $nn\gamma$ reactions reduces these cross sections by an order of magnitude. The absence of charge and smaller magnetic moment will further suppress $nn\gamma$ relative to $pp\gamma$. Considering these facts it is not surprising that the first experiments bearing on nucleon bremsstrahlung were concerned with $np\gamma$ reactions.

Wilson[7] in 1952 was the first to observe p-nucleus bremsstrahlung. Cohen *et al.*[8] continued the work at higher energy using a high-resolution pair spectrometer to determine the gamma energy. Several different nuclei were examined. In view of the relative size of the expected cross sections ($\sigma_{np\gamma}/\sigma_{pp\gamma}\approx 10$), the measured rates were attributed to radiation from np interactions. The number of nucleons present in a nucleus complicates the interpretation of the data obtained since the Pauli principle and the momentum distribution of the nucleons must be properly accounted for. Beckham[9] has developed a theory for such a situation. Recently, gamma rates from collisions of protons with deuterium have been measured.[10,11] Even with a nucleus as simple

* Based on a thesis submitted by K. W. Rothe in partial fulfillment of the Ph.D. degree at the University of Rochester. Supported by U. S. Atomic Energy Commission. This article is more detailed than preliminary reports (Ref. 25) and corrects some errors made in them.

† Present address: University of Pennsylvania, Philadelphia, Pennsylvania.

‡ Present address: University of Maryland, College Park, Maryland.

[1] R. Wilson, *The Nucleon-Nucleon Interaction* (John Wiley & Sons, Inc., New York, 1963).

[2] K. E. Lassila, M. H. Hull, Jr., H. M. Ruppel, F. A. McDonald, and G. Breit, Phys. Rev. **126**, 881 (1962).

[3] M. Konuma, H. Miyazama, and S. Otsuki, Progr. Theoret. Phys. (Kyoto) **19**, 17 (1958).

[4] H. Feshbach, E. Lomon, and A. Tubis, Phys. Rev. Letters **6**, 636 (1961).

[5] A. Scotti and D. Y. Wong, Phys. Rev. **138**, B145 (1965).

[6] See, for example, J. M. Blatt and V. F. Weisskopf, *Theoretical Nuclear Physics* (John Wiley & Sons, Inc., New York, 1952), p. 599.

[7] R. Wilson, Phys. Rev. **85**, 563 (1952).

[8] D. Cohen *et al.*, Phys. Rev. **130**, 1505 (1963).

[9] W. C. Beckham, thesis, University of California Radiation Laboratory Report No. UCRL 7001, 1962 (unpublished).

[10] J. A. Edgington and B. Rose, Phys. Letters **20**, 552 (1966).

[11] P. F. M. Koehler, K. W. Rothe, and E. H. Thorndike, Bull. Am. Phys. Soc. **11**, 303 (1966).

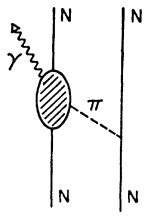

FIG. 1. Ueda's model of bremsstrahlung.

as deuterium, there are a number of possible gamma-producing channels available which are not strictly np interactions. Current experiments at Rochester will provide sufficient information on the competing channels to be able to extract a cross section for $np\gamma$.

Ashkin and Marshak[12] were the first to consider the theoretical problem of np bremsstrahlung using a semiphenomenological field theoretic potential. Simon[13] calculated the cross section for np bremsstrahlung for scalar and pseudoscalar couplings. Some work has also been done in Russia, the most recent being that of Timan[14] who includes noncentral forces in his calculations. Cutkosky[15] shows the importance of final-state interactions of the two nucleons for cases where very high-energy gamma rays are emitted. This gives rise to a peaking in the cross section as the kinematic limit of the gamma energy is approached. Using an optical model, Kurşunoğlu[16] performed an average over inelastic channels and calculated bremsstrahlung from the nucleus as a whole. Lastly, there is the more recent work of Beckham[9] mentioned above.

Theoretical work bearing on the pp bremsstrahlung reaction is of more recent vintage, aside from the initial work done by Ashkin and Marshak[12] (in whose approximation the cross section vanished). Dullemond and de Swart[17] have examined the high-energy end of the gamma spectrum via the $E2$ contribution, but have not considered the regions lower then 5 MeV from the kinematic limit. They find a peaking similar to that found by Cutkosky for the $np\gamma$ case.

The first calculations applicable to most of the γ-ray energy spectrum were those of Sobel and Cromer.[18] They describe the pp interaction by a phenomenological potential, treat the electromagnetic interaction to first order, and neglect effects of meson currents. Their recent calculations[19] show that the Breuckner-Gamel-Thaler potential gives a factor of 2 larger cross section than the Yale or Hammada-Johnston, which in turn are a factor of 4 larger than measurements at 158 and 204 MeV. Similar calculations have been carried out by Signell and Marker,[20] confirming the above results. Recently, an error in these calculations has been discovered, lowering them all by a factor of 4 and bringing them into good agreement with experiment. Duck and Pearce[21] have performed similar calculations with a Tabakin potential, getting results also in general agreement with experiment. Unfortunately, Sobel and Cromer, Signell and Marker, and Duck and Pearce all calculate cross sections for the restricted geometry in which all three final-state particles are coplanar in the lab system.

Ueda[22] has done a one-pion-exchange calculation, as illustrated in Fig. 1. The reaction is thought of as occurring via the exchange of one pion followed by a photoproduction-like vertex (the shaded area). This vertex is related to the known photoproduction amplitude by dispersion relations. The off-mass-shell nature of the exchanged pion is allowed for by a form factor taken from peripheral model calculations of Amaldi and Selleri.[23]

Any experimental approach to pp bremsstrahlung must recognize the relative smallness of the cross section (we find that the total bremsstrahlung cross section, for γ-ray energies greater than 35 MeV, is $\sim 10^{-5}$ times the total p-p elastic scattering cross section) and hence the need for good background rejection. Two approaches have been tried. Gottschalk, Shlaer, and Wang[24] at Harvard (and subsequently Warner[25] at Manitoba and Richardson *et al.*[26] at UCLA) detect both protons in small solid-angle detectors, measuring their direction and energy. The three-body final state is thus *once* overdetermined. For no apparent reason, all experiments of this sort have detected both protons at equal angles to the beam and (with one exception[27]) in a coplanar geometry. High-intensity beams are required, eliminating the possibility of using polarized beams. Our approach has been to detect the γ-ray in a small solid-angle detector, and both protons in large solid-angle detectors, obtaining the direction of all particles and the energy of the protons. Our final state is thus *three* times overdetermined, allowing excellent background rejection. We were able also to use a polarized proton beam.[28]

In summary, it may be said that N-N bremsstrahlung is in its infancy theoretically and experimentally, and

[12] J. Ashkin and R. E. Marshak, Phys. Rev. **176**, 58 (1949).
[13] A. Simon, Phys. Rev. **79**, 575 (1950).
[14] B. L. Timan, Zh. Eksperim. i Teor. Fiz. **30**, 881 (1956) [English transl.: Soviet Phys.—JETP **3**, 711 (1956)].
[15] R. E. Cutkosky, Phys. Rev. **103**, 505 (1956).
[16] B. Kurşunoğlu, Phys. Rev. **105**, 1846 (1957).
[17] C. Dullemond and J. J. de Swart, Physica **26**, 664 (1960).
[18] M. I. Sobel and A. H. Cromer, Phys. Rev. **132**, 2698 (1963).
[19] M. I. Sobel and A. H. Cromer, Phys. Rev. (to be published).
[20] P. Signell and D. Marker, Proceedings of the Williamsburg Conference on Intermediate Energy Physics, 1966, p. 657 (unpublished).
[21] I. Duck and W. A. Pearce, Phys. Letters **20**, 669 (1966).
[22] Y. Ueda, Phys. Rev. **145**, 1214 (1966).
[23] U. Amaldi and F. Selleri, Nuovo Cimento **31**, 360 (1964).
[24] B. Gottschalk, W. J. Shlaer, and K. H. Wang, Phys. Letters **16**, 294 (1964).
[25] R. E. Warner, Phys. Letters **18**, 289 (1965).
[26] R. Richardson *et al.*, Phys. Rev. Letters (to be published); Bull. Am. Phys. Soc. **11**, 302 (1966).
[27] B. Gottschalk, W. J. Shlaer, and K. H. Wang, Nucl. Phys. (to be published).
[28] K. W. Rothe, P. F. M. Koehler, and E. H. Thorndike, Phys. Rev. Letters **16**, 1120 (1966); Proceedings of the Williamsburg Conference on Intermediate Energy Physics, 1966, p. 677 (unpublished).

that as a field it promises to provide quite sensitive tests for models of the two-nucleon interaction in the intermediate energy domain.

In Sec. II we discuss the experimental apparatus, its calibration and use. Data reduction is discussed in Sec. III while the analysis and results are given in Sec. IV. Finally, a summary of the important results is given in the concluding section (Sec. V).

II. EXPERIMENTAL

General Comments

The experimental layout is shown in Fig. 2. The two threshold gamma detectors (GR, GL) gave good information on the gamma direction ($\pm 8°$ half-width at half maximum, HWHM) and set a lower limit of 20 MeV on the energy of any gamma rays seen. A pair of large scintillation counters (5,6) were set on either side of the beam to detect forward scattered protons. A $\gamma 56$ coincidence acted as a trigger for the direction and range spark chambers (DN, DS, RN, RS) which were placed closely behind the proton counters. The measurements of the direction and range of both protons were sufficient to tie down each event very well. Two gamma detectors were used to speed up data collection. They were placed at equal angles to the beam so that asymmetries in the gamma-ray distribution due to incident beam polarization were directly measured. In addition to true coincidence triggers, delayed trigger channels were set up so that, simultaneously with good data, random coincidence data could be taken.

Beam and Beam Monitoring

The external polarized beam of the University of Rochester 130-in. cyclotron was used for this experiment. It was 90% polarized up and was transported to the experimental area through a quadrupole and bending magnet combination which together with the fringing field of the cyclotron provided horizontal and vertical focusing. On exiting from the bending magnet, the beam size was trimmed by the brass slits. In order not to flood the chambers with elastically scattered proton tracks, it was necessary to use the "cee" (auxiliary dee) to improve the effective duty cycle from 1% to about 30%. While taking data, approximately 1.8×10^7 protons/sec were incident on the target with a mean energy[29] at the target of 204 MeV and a width (HWHM) of ± 6 MeV (including target thickness).

All coincidence circuits were gated off during that part of the fm cycle when the prompt-beam spike would normally occur. Taking pictures of chambers flooded with elastic events was thus avoided. Beam losses due to gating were determined simultaneously with all data. Typical losses were 15%.

The beam intensity was monitored by use of an ion chamber downstream of the chambers through which the unscattered beam was allowed to pass by opening a 3-in. gap between the two proton chambers. (The presence of this gap, together with the requirement of detecting one proton on either side of the beam, introduced the need for a correction in the measured cross sections for protons scattering into the gap or with both into the same chamber.)

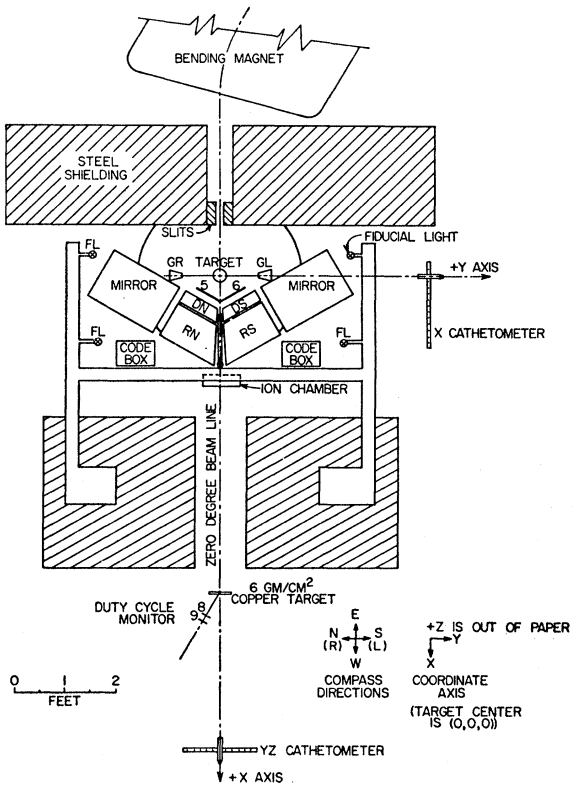

FIG. 2. Layout of experimental area.

The ion chamber was calibrated to better than 7% by using known elastic pp scattering at 20° (lab)[30] and provided the absolute monitor of the number of incident protons for the experiment.

Target

The liquid-hydrogen target was of standard cryogenic design. The cup was a 3-in.-diameter vertical cylinder 3-in. high made of 0.003-in. Mylar with brass rims to give it structure. The vacuum jacket surrounding the cup was made from $\frac{1}{32}$-in.-wall aluminum cylinder. The wall was made thin for three reasons:

(1) To minimize range losses of lower energy protons from the $pp\gamma$ reaction.

(2) To reduce to a minimum the number of gamma rays converted before they reached the gamma detector

[29] M. Rich and R. Madey, University of California Radiation Laboratory Report No. UCRL-2301 (unpublished).

[30] The 20° cross section and polarization data used was taken from recent measurements of J. F. Marshall, thesis, University of Rochester, 1966 (unpublished).

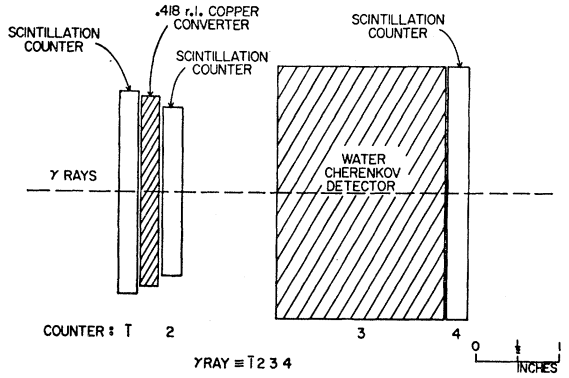

FIG. 3. Gamma counter.

($\frac{1}{32}$-in. Al=0.0099 radiation length (r.l.), while the detector was 0.418 r.l.).

(3) To reduce p-nucleus bremsstrahlung and π^0 production in the walls by elastically scattered protons.

The direct beam passed through windows made of 0.005-in. Mylar and thus encountered little material in its path.

Gamma-Ray Detector

Tests of a number of gamma counters led to the adoption of the design illustrated in Fig. 3. In order to be counted, a particle had to enter as neutral ($\bar{1}$), convert in the 0.42-r.l. copper converter, producing charged particles which counted in scintillator 2, water threshold Čerenkov counter 3, and scintillator 4. The counter was tuned so that it was only necessary for one charged particle to reach counter 4.

The Čerenkov counter with threshold $\beta=0.75$ effectively rejected all protons since $\beta=0.61$ for 210-MeV protons. Proton rejection by the Čerenkov counter was shown to be better than 10^{-5} by placing the counter in the direct beam at reduced intensity. The counter apparently had some sensitivity to slow neutrons. In the application of the counter to this experiment a false "gamma" background introduced random coincidences with 5 and 6. From analysis of the chamber pictures, these occurrences were eliminated. Delayed coincidences taken simultaneously with the data showed the random rate to be never larger than 10% of the total rate.

To be able to calculate cross sections, it was necessary to know the efficiency of the gamma detector as a function of gamma energy. The low-energy cutoff of the gamma-ray efficiency curve (see Fig. 4) was determined primarily by the ionization losses for the higher energy electron of the pair. These losses continue to affect the efficiency considerably up to 80 MeV. Outscattering by the converter and water, and bremsstrahlung losses, have a significant effect at energies as high as 200 MeV. The maximum gamma-ray energy seen in the $pp\gamma$ reaction in this experiment was 115 MeV. Hence, an adequate estimate had to treat radiative processes and multiple scattering carefully. This estimate was obtained by randomizing conversion, scattering, and radiative processes by means of a Monte-Carlo procedure. The resulting efficiency as a function of gamma ray energy is shown in Fig. 4.

As a check on the calculated efficiency, a calibration at the Cornell 1.8-BeV synchrotron using tagged photons of known energy was performed. Points at 50-, 100-, 150-, and 200-MeV gamma energy were taken. These are plotted on the efficiency curve as (0). They have been normalized such that the 200-MeV point agrees with the predicted value. Although the over-all normalization of our data taken at Cornell was not known, the experimental limits within which the points had to lie (shown as "$-L$") always spanned the calculated curve. The agreement in shape is excellent.

Proton Spark Chambers and Optics

Figure 2 indicates the size of the chambers and their positions. The direction chambers presented a minimum amount of material to the protons (0.001-in. of aluminum per foil) and allowed determination of directions. Multiple scattering and range losses in these chambers were small compared to the $\frac{1}{32}$-in. aluminum wall of the vacuum jacket and the hydrogen in the cup. The four active gaps of each direction chamber were independently fed, resulting in an efficiency for each gap close to 100%.

The range chambers were constructed of copper and aluminum plates of varying thicknesses. The first plate set a lower limit of about 60 MeV on the protons which could enter the first gap. (This depended somewhat on the angle the particle track made to the plates.) The target thickness introduced sufficient uncertainty in the particle range for protons of less than 60 MeV so that little use could have been made of range data taken on these particles. The remainder of the plates of the range chambers were chosen to give approximately 10% energy resolution for protons above this lower energy limit. All the information required for a given event was recorded on one 1-in.×2-in. picture using 35-mm film.

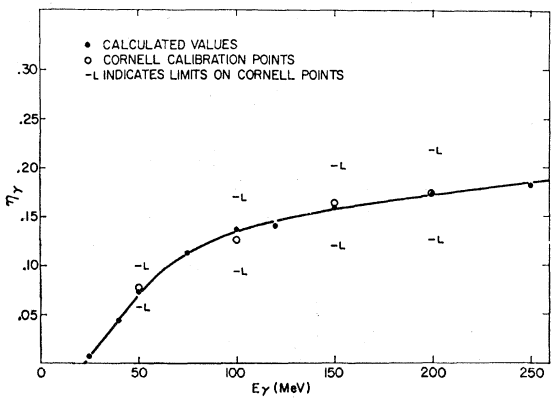

FIG. 4. Gamma-counter efficiency as a function of gamma energy.

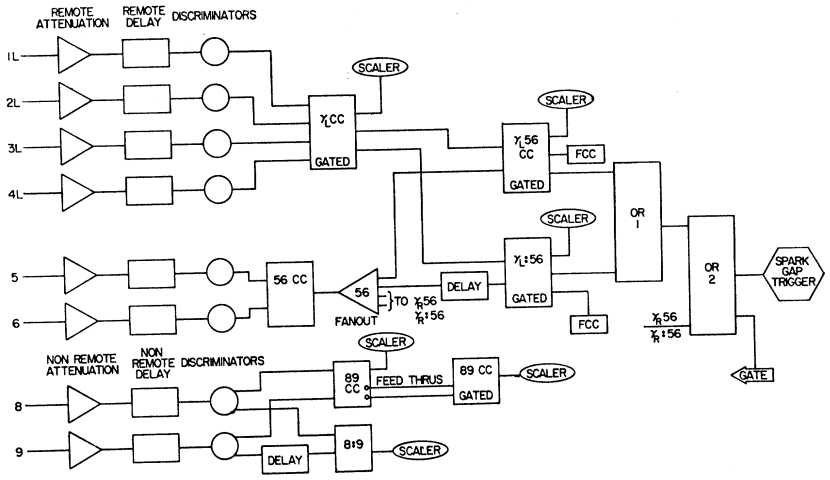

FIG. 5. Electronic logic. 8 and 9 are duty-cycle monitor counters.

The camera was suspended 15 ft above the chambers with its optic axis vertical. It employed a 135-mm focal length lens. One mirror looked into each set of chambers (north and south), giving 90° stereo views of each spark. The position of the camera allowed viewing directly down each direction chamber gap. Prisms were required, however, to see the full depth of each range gap.

Electronics

Figure 5 indicates the electronic logic used in the experiment. All logic circuitry was of standard Chronetics modular type.

Run Procedure

Table I indicates the amount of time spent at each of the three gamma angles. In all cases, the two gamma detectors were at equal angles to the beam and on opposite sides of it (i.e., one north and one south). The gamma detectors were frequently interchanged to average over any differences that might exist between counters. For each gamma-ray angle, half of the data were taken in each configuration. Most of the data were taken at center-of-mass angles of 108° and 146°, only ~10% being 59½° data. The 59½° case was complicated by the fact that only direction chambers were used (the range chambers having been rolled back on trolleys), and the solid angles of the gamma counters were reduced by a factor of 3. Consequently, the signal-to-background picture ratio was poorer.

TABLE I. Picture summary.

θ_γ[a]	Protons	Pictures	% random	% 2-prong	% 2-prong random	% $pp\gamma$
59½° full	8.4×10^{11}	251	9.1	35.5%	3.6%	18%
59½° empty	1.1×10^{11}	44	10.0	16.5	2.0	2
108° full	2.9×10^{12}	1308	4.8	52.5	2.1	24
108° empty	3.0×10^{11}	55	6.1	25.0	0	1.8
146° full	1.7×10^{12}	591	7.3	47.5	2.3	21
146° empty	1.6×10^{11}	29	9.4	12.5	0	0

[a] These angles refer to the center of mass of the $pp\gamma$ system.

In addition to the sets of data taken with the target full, a little more than one-tenth of the data-collection time was spent taking target-empty data. Periodic pp elastic events were interspersed with the bremsstrahlung sets. These pictures gave assurance of good chamber operation and provided checks of track measurement and reconstruction errors. Film processing was such that within 24 h of taking a given data set, the pictures were available to be scanned. This allowed continuous monitoring of the whole experimental situation. The scanned film gave the number of two track possibilities immediately and helped to determine the length of time required for each phase of data collection.

III. DATA REDUCTION

As seen in Table I, roughly one-half of the pictures did not contain two-proton prongs and could be discarded at the scanning table. (Approximately 80% of these triggers were to be expected from the target-empty and delayed coincidence rates.) The two-prong events were measured and fitted to the hypothesis of pp bremsstrahlung, as described below. Again, about one-half did not fit. This number can be broken down into 9% randoms, 19% target-empty, 20% "walls," and 7% unexplained. (By "walls" is meant a pp elastic scattering in hydrogen, followed by a p-nucleus bremsstrahlung or π^0 production in the target walls, giving rise to a two-prong event with a γ ray. It was calculated to be $20\pm4\%$ of the two-prong rate, and is readily separated from pp bremsstrahlung by the fitting procedures.)

The primary tool used to discriminate $pp\gamma$ events from background was a routine which tried to fit the measured kinematic quantities of each pair of tracks and the γ ray direction to the hypothesis of pp bremsstrahlung. The fitting parameter that was minimized

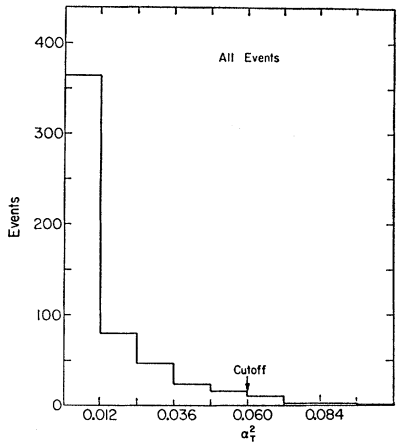

FIG. 6. α_t^2 (fitting parameter) distribution.

was:

$$\alpha_t^2=\sum_{1,2}2(1-\cos\beta_i)+0.005\left(\frac{T_{i(\text{measured})}-T_{i(\text{predicted})}}{T_{i(\text{predicted})}}\right)^2,$$

where β_i is the space angle between predicted and measured momentum of the ith proton, the T_i is its kinetic energy. This form gives somewhat less weight to energy measurements than their errors would warrant, but eliminates false fits in which one proton is assigned essentially zero momentum and hence arbitrary direction.

On the basis of the minimum value for each event, it was possible to place it in one of three groups. The first contained those events which had very large values and could be rejected immediately, such values being inconsistent with known or estimated measuring accuracy. These events formed a very long flat tail in the α_t^2 distribution. The second group lay within the peak region and formed the bulk of what were taken as good events (i.e., they fit bremsstrahlung well). The third region corresponded to the merging of the tail of the good event distribution with the flat, nonbremsstrahlung background tail. A cut was made in this region beyond which events were rejected. This cut was arbitrary, but all quoted angular distributions were shown to be independent of its position and errors in the final cross sections have been increased to account for this arbitrariness. Figure 6 shows the α_t^2 distribution and the location of the cut. The bulk of the rejected data is off scale to the right.

Having thus picked those events consistent with the bremsstrahlung hypothesis (and obtained best-fit values for all the kinematic variables), a further selection criterion was imposed. This was to ask of each event that its reconstructed interaction vertex be spatially consistent with the known target and beam dimensions. Only events passing this test were kept as bremsstrahlung; this eliminated 8% of the previously surviving sample.

In addition to analyzing those events which were indicated by code lights as true coincidences, those which were taken as the result of a delayed coincidence trigger were analyzed. The α_t^2 distribution for this group of events was flat showing no peaking in the region of small values. A further illustration of where random event pictures might fall was gathered by pairing tracks from different pictures. This again gave a flat distribution. The same held true for those pictures taken with the target empty. We were thus quite confident that the normal sources of events which come disguised as true events contribute no more to the peak region than to the tail.

IV. DATA ANALYSIS AND RESULTS

Kinematic Considerations

The final state in the pp bremsstrahlung reaction has three particles present; it follows that the most multiply-differential cross section attainable is $d^5\sigma$ (calling $d\Omega=\sin\theta d\theta d\phi$ to give 2), where one is free to choose the five variables with respect to which it is differentiated from among the energies and directions of the final state particles; or, as will be done here, some combination of these variables which seems to be the physically most meaningful can be chosen. pp elastic scattering is normally described in the two-body center-of-mass system. The protons come off back to back and the angles $\theta_{\text{c.m.}}$, $\phi_{\text{c.m.}}$ are well defined (where θ is the polar angle with respect to the incoming direction and ϕ the azimuth). It seemed appropriate in the case of pp bremsstrahlung to define a similar pair of c.m. angles such that, in the limit as the gamma-ray energy approaches zero, they reduce to the elastic-scattering c.m. angles. To do this, a momentum-averaged pair of scattering angles in final three-body (or initial two-body) c.m. system was defined. They are illustrated in Fig. 7. The two angles are:

$$\cos\theta_{\text{c.m.}}=\frac{(\mathbf{P}_{1C}-\mathbf{P}_{2C})}{|\mathbf{P}_{1C}-\mathbf{P}_{2C}|}\cdot\hat{\imath},$$

$$\cos\phi_{\text{c.m.}}=\frac{(\mathbf{P}_{1C}-\mathbf{P}_{2C})}{|\mathbf{P}_{1C}-\mathbf{P}_{2C}|\sin\theta_{\text{c.m.}}}\cdot\hat{\jmath}.$$

The other three variables were taken as E_γ, θ_γ, ϕ_γ, the energy and direction of the γ ray in the final three-body c.m. system.

Polar angles are defined so that $\theta=0°$ along the beam line. Azimuthal angles are defined so that $\phi=0$, 180° in the horizontal plane. It should be noted that with our definition of ϕ, the experimental setup was such that either $\phi_\gamma=0°$ (gamma detector south of beam) or 180° (gamma detector north of beam).

For proton center-of-mass angular distributions, we have chosen to combine the data obtained with the gamma counters on either side of the beam. In so doing, we are averaging over incident-beam polarization effects.

Only the first quadrant of the $\phi_{c.m.}$ distributions has been plotted with all $\phi_{c.m.}>\pi/2$ folded into it in the usual way:

$$\phi_{c.m.}\rightarrow\pi-\phi_{c.m.} \quad \text{for} \quad \pi\geqslant\phi_{c.m.}>\pi/2,$$
$$\phi_{c.m.}\rightarrow\phi_{c.m.}-\pi \quad \text{for} \quad 3\pi/2\geqslant\phi_{c.m.}>\pi,$$
$$\phi_{c.m.}\rightarrow 2\pi-\phi_{c.m.} \quad \text{for} \quad 2\pi\geqslant\phi_{c.m.}>3\pi/2.$$

In so doing, we have assumed that the combined gamma data are symmetric about both the $\phi=0$, and the $\phi=\pi/2$ axes. This fact is pointed out by the following considerations:

(1) The gamma rays always come out in the plane containing $\phi=0$ and π.

(2) With an unpolarized beam (or summing over $\phi_\gamma=0$, π), there can be no distinction between the octants with $\pi/2\geqslant\phi_{c.m.}>3\pi/2$ and those with $3\pi/2\geqslant\phi_{c.m.}>\pi/2$. Thus, we may fold about $\phi=\pi/2$.

(3) For each gamma which has $\phi_\gamma=0$ and a given $\phi_{c.m.}$ there is a conjugate-gamma possibility with $\phi_\gamma=\pi$ and $\phi_{c.m.}=\pi+\phi_{c.m.}$. We are thus free to fold about the $\phi=\pi$ axis.

The $\theta_{c.m.}$ data are presented in the first quadrant only (rather than the first two). This can be done since the two protons are identical particles and the transformation $\theta_{c.m.}\rightarrow\pi-\theta_{c.m.}$, $\phi_{c.m.}\rightarrow\pi+\phi_{c.m.}$ cannot change cross sections.

Corrections and Errors

Only those events which gave one proton in each chamber (north and south) were accepted for analysis. Therefore, it was necessary to correct or reinterpret all distributions and cross sections to allow for cases where one of the protons did not head towards a chamber or had insufficient energy (<35 MeV) to reach a chamber, and for cases, frequent at high γ-ray energies, where both protons entered the same chamber. The angular region $1.0\geqslant\cos\theta_{c.m.}\geqslant 0.65$ was not detected because one proton had insufficient energy; the region $90°\geqslant\phi_{c.m.}\gtrsim 65°$ was missed because a proton missed its chamber, either going over the top or into the gap between the chambers; the region 85 MeV$\lesssim E_\gamma\leqslant E_\gamma^{max}$ was missed because both protons were on the same side of the beam.

Corrections were obtained by a Monte Carlo calculational procedure. "Fake" events were randomly generated, according to various assumed distributions in $\cos\theta_{c.m.}$, $\phi_{c.m.}$, and E_γ. A "measured" range was calculated for each event by picking an interaction point randomly within the target, and allowing for the finite plate thickness of the range chambers. For each event classified as a "hit" (one particle in each direction chamber), "measured" directions were calculated by randomly smearing vertical and horizontal projections of the angles of both particles. The "fake" event thus generated was fitted by the same program used on actual events. A smearing of ±4° rms in projected angles, although twice what we had estimated from measuring accuracy, gave an α_t^2 distribution with the same width as that of the actual events, and hence was used for all corrections. Root-mean-square deviations of fitted values of $\cos\theta_{c.m.}$, $\phi_{c.m.}$, and E_γ from the unsmeared values were found to be ±0.2, ±7°, and ±7 MeV, suggesting similar uncertainties in the fits to the actual data.

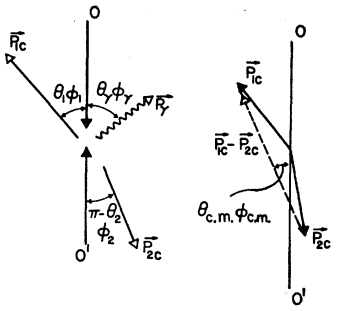

FIG. 7. Definition of proton center-of-mass scattering angles. OO' is the beam line.

The "fake" data are used in two ways: (1) Histograms of fake data with various assumptions about the distributions in $\cos\theta_{c.m.}$, $\phi_{c.m.}$, are compared against actual data, thus testing the ability of the data to differentiate among the assumed distributions. (2) The ratio of "hits" to all generated events is used to correct cross sections for missed events. Uncertainty in this correction is the dominant error in the cross sections $d\sigma/d\Omega_\gamma$.

The procedure described above had not been carried out when the preliminary descriptions[25] of this experiment were presented. Further, in the less detailed analysis used at that time, the minimum proton energy required for detection had been incorrectly taken too low. As a result, erroneous conclusions were reached concerning the cross section $d\sigma/d\Omega_\gamma$ and distributions in $\cos\theta_{c.m.}$ and $\phi_{c.m.}$.

The ion chamber used to monitor the incident protons was calibrated twice during the final data run. It had been also calibrated several times prior to the run. The different values obtained agreed to within the error indicated and gave one electrometer pulse= $(1.76\pm0.12)\times10^7$ protons. The likelihood was small of there being short-term changes large compared to this 7% error for this instrument, and the quoted error was taken as the over-all rms variation.

The effective target thickness was calculated by combining measurements made on the beam profiles with the known physical dimensions of the cup. Short-term variations in the position of the beam centroid due to current fluctuations in the bending magnet introduced an error in the target thickness of less than 1%.

A further effect due to centroid changes appears as a false gamma-ray asymmetry: A centroid shift increases the solid angle for one gamma counter while reducing it for the other. We estimate this to alter solid angles by 0.5% (small compared to the statistical errors on the asymmetries). This error tends to average out in time since the beam wandered both left and right.

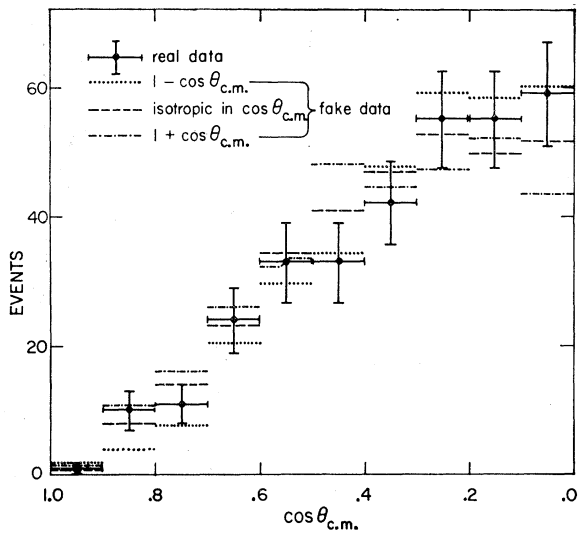

FIG. 8. Distribution of events as a function of $\cos\theta_{c.m.}$, for $\theta_\gamma=108°$. Shown are the experimental points, and histograms of "fake" data for three assumed distributions.

In addition to beam wandering, one had to consider the possibility of the beam centroid and the target center not coinciding. The gamma counters were positioned relative to the target and not the beam. A systematic uncertainty in gamma asymmetry of 0.02 was thus present.

We consider now those corrections arising from the extraction of data from the spark-chamber pictures. Scanning efficiency has been estimated to be $(98\pm1)\%$. Some events were lost as a result of the chambers being unable to handle multiple tracks. Since only one out of ten of the two-track pictures contained three or more tracks, and loss of sparking efficiency was not frequently apparent, a reasonable estimate placed this at a $(3\pm1)\%$ correction. Within the peak regions in the α_t^2 distribution from the fitting program a certain number of background events were included, and, although one could not determine which events should be excluded on an individual basis, projection from the tail of poor fits gave a $(3\pm1)\%$ correction for $\theta_\gamma=108°$, 146°. At $\theta_\gamma=59\frac{1}{2}°$ the background was higher and the correction was estimated at $5\pm5\%$. The various sources of systematic error are summarized in Table II.

Results

As a consequence of having completely determined all kinematic quantities for each bremsstrahlung event, we are in a position to provide information on several aspects of the reaction. Data concerning $(d^2\sigma/d\Omega_\gamma dE_\gamma)$, $d\sigma/d\Omega_\gamma$, and angular distributions of events in $\cos\theta_{c.m.}$ and $\phi_{c.m.}$ will be presented as well as proton and gamma-ray asymmetries due to having an initially polarized beam. In addition, an invariant-mass spectrum for $m_{\gamma+p}$ will be given which may be regarded as a search for an excited proton state which decays into

TABLE II. Systematic errors.[a]

Source	Error (%)
Ion-chamber normalization	7
Gamma efficiency	6
Proton-efficiency correction	20
Scanning efficiency	1
Background in α_t^2 peak	1
Multitrack picture efficiency	1
Total rms error	22%

[a] At $\theta_\gamma=59\frac{1}{2}°$ the background-correction error → 5%. The gamma efficiency error represents that change in local gamma efficiency which could be made without grossly distorting the general shape of the calculated curve.

a proton and a gamma ray:

$$p+p\rightarrow p+p^*$$
$$\searrow$$
$$p+\gamma.$$

Finally, by transforming our cross sections through the appropriate Jacobian we obtain a comparison with the work of others who have measured $(d^2\sigma/d\Omega_1 d\Omega_2)_{lab}$.

Proton Center-of-Mass Angular Distributions

Figure 8 shows the distribution of events as a function of $\cos\theta_{c.m.}$ for $\theta_\gamma=108°$. Distributions obtained at $\theta_\gamma=59\frac{1}{2}°$ and 146° showed similar features but had poorer statistics. Also shown in the figure are histograms of "fake" events generated according to three assumed distributions in $\cos\theta_{c.m.}$: $1-|\cos\theta_{c.m.}|$, isotropic in $\cos\theta_{c.m.}$, $1+|\cos\theta_{c.m.}|$. (It should be noted that the first and last of these do not correspond to proper physical behavior, in that $|\cos\theta_{c.m.}|$ is not a smooth function. These distributions have been used only for convenience to give peaking near $|\cos\theta|=0$, and near $|\cos\theta|=1$, respectively. A smoothed out distribution with the same general peaking would give the same histogram.) The shape of the "fake" histograms in $\cos\theta_{c.m.}$ is insensitive to the assumed $\phi_{c.m.}$ distribution; the distribution $1+\frac{3}{2}\cos^2\phi_{c.m.}$ was used. The histograms of "fake" events have been normalized to the same number of events as the real events. We ran typically four times as many fake events for each distribution, as real events, and hence statistics on the fake histograms are unimportant.

The gross features of Fig. 8 are of an instrumental nature, as is demonstrated by the similarity between the histograms for "fake" events of different distributions. Detection efficiency, which is fairly constant in the region $0\leqslant\cos\theta_{c.m.}\leqslant0.6$, drops to zero between $\cos\theta_{c.m.}=0.6$ and 0.7. However, because $\cos\theta_{c.m.}$ is only determined to ±0.2, the sharp drop is smeared out, giving a smooth decrease to zero as $\cos\theta_{c.m.}$ increases.

By comparing the real data against the "fake," in the region $0\leqslant\cos\theta_{c.m.}\leqslant0.3$, and in the region $0.4\leqslant\cos\theta_{c.m.}\leqslant0.7$, one concludes that $1+|\cos\theta_{c.m.}|$ is a bad representation of the data, while isotropy and $1-|\cos\theta_{c.m.}|$

are adequate representations. The average of the "$1-|\cos\theta_{c.m.}|$" and "isotropy" histograms gives an excellent fit. We conclude that there is a peaking of events near $\cos\theta_{c.m.}=0$, characterized by the distributions $[1; 1+\frac{3}{2}(1-|\cos\theta_{c.m.}|); 1-|\cos\theta_{c.m.}|]$, where the middle distribution is the best fit and the two end distributions are one standard deviation away. In our earlier publications,[25] we arrived at the erroneous conclusion that the peaking near $\cos\theta_{c.m.}=0$ was stronger and statistically more significant (see Corrections and Errors above).

Figure 9 shows the distribution of events as a function of $\phi_{c.m.}$, for $\theta_\gamma=108°$. (It should be remembered that this is also the distribution in $\phi_{c.m.}-\phi_\gamma$.) Distributions obtained at $\theta_\gamma=59\frac{1}{2}°$ and 146° showed similar features and had poorer statistics. Also shown in the figure are histograms of "fake" events generated according to two assumed distributions in $\phi_{c.m.}$: isotropic in $\phi_{c.m.}$, and $\cos^2\phi_{c.m.}$. The shape of the "fake" histograms in $\phi_{c.m.}$ is insensitive to the assumed $\cos\theta_{c.m.}$ distribution; the distribution $1+\frac{3}{2}(1-|\cos\theta_{c.m.}|)$ was used. The histograms of "fake" events were obtained from typically 4 times as many events as the real events, and have been normalized to the same number of events.

The decrease in events as $\phi_{c.m.}$ increases is in part instrumental, as detection efficiency drops to zero in the region 50° to 70°. However, by considering the ratio of events in the regions $40°\leqslant\phi_{c.m.}\leqslant70°$ and

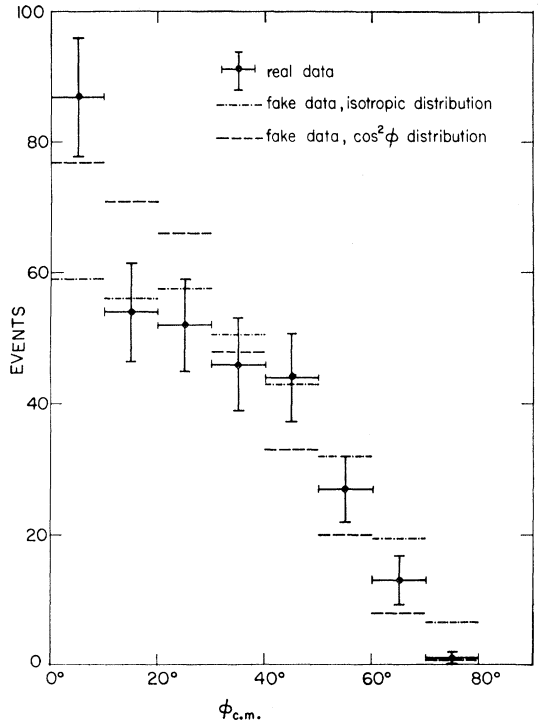

FIG. 9. Distribution of events as a function of $\phi_{c.m.}$, for $\theta_\gamma=108°$. Shown are the experimental points, and histograms of "fake" data for two assumed distributions.

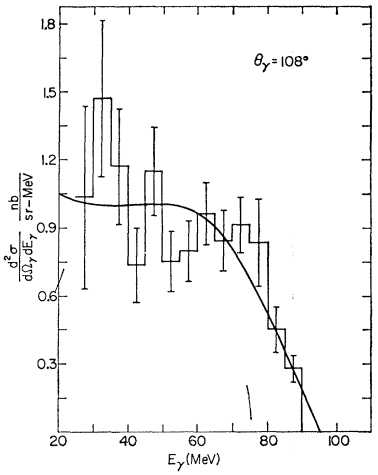

FIG. 10. Cross sections $d^2\sigma/d\Omega_\gamma dE_\gamma$ versus E_γ, at $\theta_\gamma=108°$. The curve is that predicted by Ueda (Ref. 22), scaled down by a factor of 1.7.

$0°\leqslant\phi_{c.m.}\leqslant30°$, one sees that the data are not consistent with isotropy, nor are they as strongly peaked near $\phi_{c.m.}=0°$ as $\cos^2\phi_{c.m.}$ would predict. The average of the two histograms fits the ratio well, though it does not fit the shape in the 0°–30° region. Specifically, the tendency for peaking near 0° is due entirely to an excess of events in the region $0°\leqslant\phi_{c.m.}\leqslant10°$; this same phenomenon is observed for $\theta_\gamma=59\frac{1}{2}°$ and 146°. Combining all three gamma angles, the excess in the region $0°\leqslant\phi_{c.m.}\leqslant10°$ over a smooth curve through the other bins is 35% of the smooth curve, a 3-standard-deviation effect. While this behavior is admittedly odd, we find no technical reason to suspect the data in the region $0\leqslant\phi_{c.m.}\leqslant10°$. They do have somewhat higher γ-ray energy than average.

A small amount of data was taken with the γ counter at $\theta_\gamma=108°$, $\phi_\gamma=270°$, thus having good detection efficiency in the region $|\phi_{c.m.}-\phi_\gamma|=90°\pm20°$, and low efficiency elsewhere. These data were collected in a later run, incidental to the main purpose of that run, and with spark chambers subtending a smaller solid angle than those of the main run. For distributions of the form $\cos^2(\phi_{c.m.}-\phi_\gamma)$; $1+\frac{3}{2}\cos^2(\phi_{c.m.}-\phi_\gamma)$, and isotropic in $\phi_{c.m.}-\phi_\gamma$, we anticipated 1.5, 6, and 11 events, respectively. We observed seven events.

We conclude that the general 0°–90° behavior of the data is adequately described by the distribution $1+\frac{3}{2}\cos^2(\phi_{c.m.}-\phi_\gamma)$, although the detailed shape is better described by an isotropic distribution with a 35% enhancement in the region $0°\leqslant|\phi_{c.m.}-\phi_\gamma|\leqslant10°$. We can find no experimental reason to discard this enhancement as spurious. In our earlier publication,[25] we arrived at the erroneous conclusion that the peaking near $\phi_{c.m.}-\phi_\gamma=0$ was stronger and statistically more significant (see Corrections and Errors above).

Cross Sections

Since the cross section $d^2\sigma/d\Omega_\gamma dE_\gamma$ is obtained by integrating $d^3\sigma/d\Omega_\gamma dE_\gamma d\Omega_{c.m.}$ over $d\Omega_{c.m.}$, one must assume a distribution in $\theta_{c.m.}$ and $\phi_{c.m.}$ to calculate the

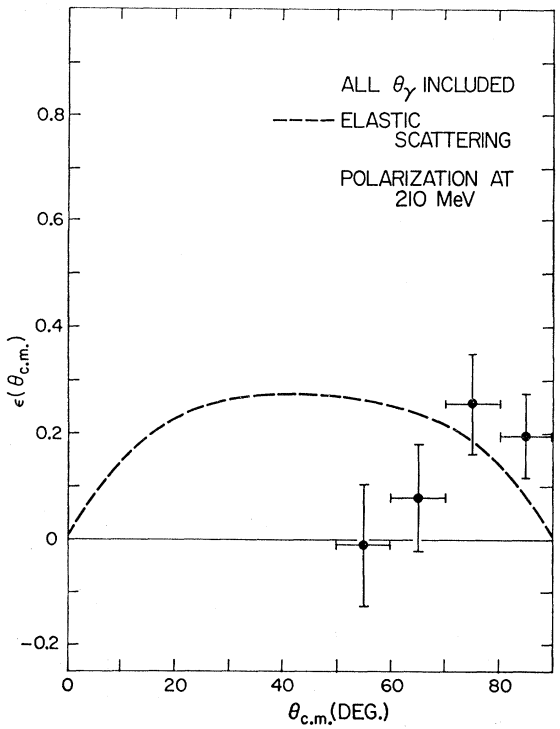

FIG. 11. Proton asymmetries. Events from $\theta_\gamma = 59\frac{1}{2}°$, 108°, and 146° have been combined. The curve is the polarization parameter in p-p elastic scattering at 210 MeV.

number of events not detected. We have tried the various distributions discussed in the preceding section, and find that the *shape* of the cross section (versus E_γ) is the same for all of them. The magnitude of the cross section, however, varies by a factor of 2 between extreme assumptions. To obtain the magnitude of the cross section, we have used the distribution

$$[1+\tfrac{3}{2}(1-|\cos\theta_{c.m.}|)]\times[1+\tfrac{3}{2}\cos^2(\phi_{c.m.}-\phi_\gamma)].$$

A $\pm 20\%$ error is assigned to the magnitude of the cross sections, to allow for the uncertainty in the choice of distribution.

The cross section $d^2\sigma/d\Omega_\gamma dE_\gamma$, at $\theta_\gamma = 108°$, is shown as a function of E_γ in Fig. 10. Results at $\theta_\gamma = 59\frac{1}{2}°$ and 146° showed the same shape with poorer statistics. The high-energy bins have been corrected as if the actual

TABLE III. Cross sections $(d\sigma/d\Omega_\gamma)_{E_\gamma \geq 35\ \text{Mev}}$.

θ_γ	$(d\sigma/d\Omega_\gamma)$ nb/sr[a]	$(d\sigma/d\Omega_\gamma)_{\text{Ueda}}$	$\left(\frac{d\sigma}{d\Omega_\gamma}\right)_{\text{Ueda}} \Big/ \left(\frac{d\sigma}{d\Omega_\gamma}\right)_{\text{exp}}$
59.5°	42.0±6.2	99.3	2.35
108°	48.0±2.7	77.1	1.59
146°	73.0±7.4	129.0	1.75
	$\sigma_{\text{total}} = 0.70 \pm 0.15\ \mu b$		

[a] In addition to the random error shown for the values of $d\sigma/d\Omega_\gamma$, there is a systematic error of 22%. This error *has* been included in the indicated error to σ_{total}.

TABLE IV. Proton asymmetries as a function of $\theta_{c.m.}$ normalized to 100% incident polarized beam.

θ_γ	$\theta_{c.m.}$	$\epsilon = (L-R)/(L+R)$	$\Delta\epsilon$
59.5°	30–60	0.555	0.340
	60–90	0.696	0.197
	All	0.167	0.173
108°	30–45	0.111	0.247
	45–60	−0.097	0.144
	60–75	0.408	0.106
	75–90	0.168	0.090
	All	0.190	0.061
146°	30–45	0.428	0.284
	45–60	0.222	0.219
	60–75	0.151	0.166
	75–90	0.265	0.137
	All	0.260	0.090
All	30–40	0.588	0.230
	40–50	0.124	0.183
	50–60	−0.016	0.132
	60–70	0.080	0.112
	70–80	0.258	0.090
	80–90	0.196	0.088
	All	0.210	0.048

cross section falls smoothly to zero at the kinematic limit. Events in the top 5 MeV are not shown as detection efficiency is zero here. The curve shown is that predicted by Ueda,[22] scaled down by a factor of 1.7. The agreement is good.

The cross section $d\sigma/d\Omega_\gamma$ was obtained by integrating $d^2\sigma/d\Omega_\gamma dE_\gamma$ from 35 MeV to the upper limit. The cross section became very uncertain below 35 MeV, because the γ detection efficiency was small and poorly known, hence the cutoff at 35 MeV. Table III gives the values of $d\sigma/d\Omega_\gamma$ with statistical error. Also included are the values which Ueda[22] predicts, and the ratio of theory to measurement which is roughly 2.

A total cross section for pp bremsstrahlung with $E_\gamma \geq 35$ MeV has been obtained by fitting a smooth curve through the three values of $d\sigma/d\Omega_\gamma$ versus θ_γ, imposing the requirement of symmetry about the point $\theta_\gamma = 90°$. We find $\sigma_{\text{total}}(E_\gamma \geq 35\ \text{MeV}) = 0.70 \pm 0.15\ \mu$b. The quoted error includes the systematic error in the $d\sigma/d\Omega_\gamma$ values, and a contribution to allow for the non-uniqueness in the smooth curve drawn through the 3 data points.

Proton and Gamma-Ray Asymmetries

Table IV shows all of the observed proton asymmetries as a function of $\theta_{c.m.}$ for the three gamma angles. These asymmetries have been normalized to a 100% polarized incident beam. Scattering right and left (R,L) are defined in the conventional way common to elastic scattering. Scattering left thus refers to the octants with $(0° \leq \theta_{c.m.} < 90°,\ 270° \leq \phi_{c.m.} < 90°)$ and $(90° \leq \theta_{c.m.} \leq 180°,\ 90° \leq \phi_{c.m.} < 270°)$ while scattering right refers to the other four octants. Detection efficiency was essentially zero for $\theta_{c.m.} < 50°$, and events with fitted angles in this region are spillover from larger $\theta_{c.m.}$ due to the large error in the $\theta_{c.m.}$ determination. The average polarization is positive for all three γ-ray angles. Figure 11 shows the results of combining the data for

TABLE V. Gamma-ray asymmetries normalized to 100% polarized incident beam.[a]

θ_γ	$\epsilon=(L-R)/(L+R)$	$\Delta\epsilon=[(1-\epsilon^2)/(L+R)]^{\frac{1}{2}}$
59.5°	0.110	0.175
108°	−0.192	0.061
146°	−0.135	0.091
All	−0.162	0.049

[a] All asymmetries are subject to a ±0.02 systematic error in addition to the statistical errors.

the three angles. A curve of the polarization parameter for elastic p-p scattering[1] at 210 MeV is given for comparison. There is agreement in sign and magnitude.

The gamma-ray asymmetries (normalized to 100% incident beam polarization) as a function of θ_γ are given in Table V. Here the sign convention used is that scattering left (L) is in the same sense as the scattering which produces the initial beam polarization, i.e., such that $\mathbf{P}_{\text{inc}}\times\mathbf{P}_\gamma$ (where $\mathbf{P}_{\text{inc}}$ is the incoming polarized beam) is parallel to the beam polarization. This corresponds to scattering south in the laboratory. The asymmetries for 108° and 146° are negative and the error is large enough at 59½° to be consistent with zero (or even small negative values for that matter). The average asymmetry (all events) is -0.162 ± 0.049 and is certainly nonzero and negative. There is also a systematic error of ±0.02 which has not been included in the quoted error.

The gamma-ray asymmetry data are more sparse than those pertaining to the proton asymmetries. At the angles for which data have been collected the asymmetries are all consistent with being negative (although 59½° is only so within statistics). The average asymmetry is of the same sign and general magnitude as the asymmetries observed in the $p+n\rightarrow d+\gamma$ pickup reaction at 200 MeV.[11] This value weights the $\theta_\gamma=108°$ and 146° data more heavily than the 59½° since most of the data were taken at the former angles.

Invariant-Mass Spectrum

A further way to analyze the data is to pair the gamma ray of each event with each of the outgoing protons in turn and determine the (γp) invariant mass. If a resonant proton state which is excited in pp collisions and has a mass in the region from 950 to 1050 MeV were to exist, its predominant mode of decay should be $p^*\rightarrow p+\gamma$. Its presence would be indicated by a peak in the invariant-mass spectrum above a smooth background.

Figure 12 shows the mass spectrum obtained from events taken at all gamma angles. The dashed curve is meant only to suggest the general shape of the curve; it is *not* a calculated curve.

The gamma-detection efficiency has not been folded into the data points but this has little local effect on the spectrum, providing only a general distortion of the background. As can be seen, there are no significant

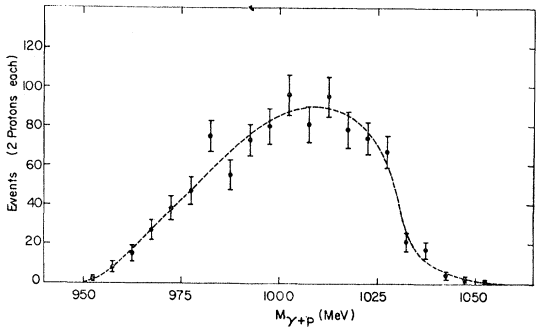

FIG. 12. (γP) invariant-mass spectrum. The dashed curve is *not* calculated and is only meant to guide the eye. Gamma efficiency has not been folded in.

deviations of the experimental points from the dashed curve.

The domain of sensitivity may be characterized by the lifetimes which could have been detected had such a resonance existed, namely $10^{-22}\leqslant\tau\leqslant10^{-10}$ sec. Here the upper limit is determined by the distance an excited proton could travel and still be fit by our fitting procedure as being from the target. The lower limit is determined by the fact that any state broad compared to 5 MeV would have been averaged into the general background. Since one would expect the $p^*\rightarrow p+\gamma$ decay to be electromagnetic, a typical decay time might be comparable to that of the π^0, or 10^{-16} sec. This falls in the center of our sensitive region. The upper limit which can be placed on the production cross section for such a resonance is 35 nb. In view of the fact that this represents about a 10^{-6} smaller cross section than that for elastic pp scattering, we conclude that it is highly improbable that any such p^* state exists at all. Examination of the Harvard data also shows no resonant behavior in the region of sensitivity $1050\geqslant m_{\gamma+p}\geqslant950$ MeV.[27]

Comparison with Coplanar Geometry Experiments

By using the functional forms which best fit the dependence of our measured cross section on θ_γ, $\theta_{\text{c.m.}}$, $\phi_{\text{c.m.}}$, and E_γ, and by calculating the Jacobian for the transformation from $(d^3\sigma/d\Omega_\gamma dE_\gamma d\Omega_{\text{c.m.}})$ to $(d^3\sigma/d\Omega_1 d\Omega_2 dE_1)$ (where 1 and 2 refer to the protons in the laboratory), we have calculated the latter cross section at 204 MeV for the case where the two protons scatter at equal angles to the beam in the laboratory. We find 13.0 ± 2.4, 14.0 ± 2.7, and 29.0 ± 6.0 μb/(sr)^2, at 30°, 35°, and 40°, respectively. These results are plotted in Fig. 13, along with those at other energies. Most of the results of the restricted geometry experiments have been obtained with the assumption that the distribution is isotropic in $\phi_{\text{c.m.}}-\phi_\gamma$. The peaking at small values of $\phi_{\text{c.m.}}-\phi_\gamma$ indicated by our data in effect reduces the effective solid angle of finite-sized proton detectors, and would require an upward correction to the quoted cross sections. The Harvard group[30] has measured this effect

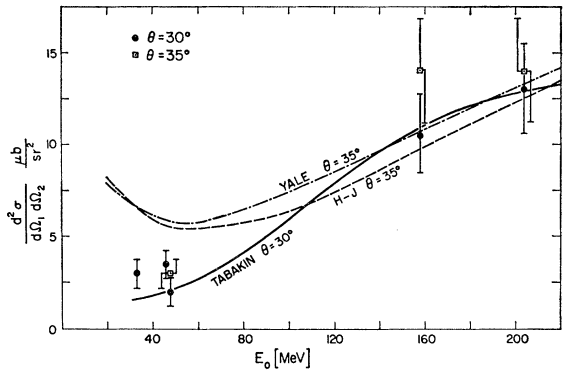

FIG. 13. $(d^2\sigma/d\Omega_1 d\Omega_2)_{\text{lab}}$ versus E_0 for restricted geometry. Solid curve is a calculation of Duck and Pearce, using the Tabakin potential. Dashed curves are calculations of Sobel and Cromer, using Yale and Hamada-Johnston potentials.

for proton angles of 30° and 35°. They also find a peaking at small $\phi_{\text{c.m.}}-\phi_\gamma$, and have corrected their 30° and 35° points accordingly. For all other points, this upward correction, of perhaps 35%, has *not* been made.

Shown also in Fig. 13 are the results of calculations of Sobel and Cromer[18] for Yale and Hammada-Johnston potentials, and of Duck and Pearce,[21] for the Tabakin potential. The initial factor of four mistakes has been removed from the former work, and some smaller calculational errors in the latter work have been corrected.[31] The agreement is now quite good. However, the $\phi_{\text{c.m.}}-\phi_\gamma$ dependence must be more thoroughly explored before one should take the agreement too seriously.

[31] W. A. Pearce and I. Duck, Bull. Am. Phys. Soc. **12**, 16 (1967); and private communication.

V. SUMMARY

Our cross sections $d^2\sigma/d\Omega_\gamma dE_\gamma$ versus E_γ agree in shape (i.e., they are flat) but disagree in magnitude with the predictions of Ueda. Proton center-of-mass angular distributions indicate a peaking near $\theta_{\text{c.m.}}=0$, and near $\phi_{\text{c.m.}}-\phi_\gamma=0$. (In laboratory coordinates, the two protons tend to have equal polar angles, and lie in the plane defined by the incident beam and the γ ray.) Proton asymmetries agree in sign and magnitude with elastic pp polarization at 210 MeV. Gamma-ray asymmetries are of the same sign and magnitude as those we have obtained in the $p+n\rightarrow d+\gamma$ measurements which in turn agree with photodisintegration calculations. We have set an upper limit of 35 nb ($\sim 10^{-6}\times\sigma_{pp\ \text{elastic}}$) on the production cross section for a resonant proton state excited in pp collisions with 950 MeV$\leqslant$mass$\leqslant$1050 MeV and 10^{-22} sec$\leqslant$lifetime$\leqslant 10^{-10}$ sec. Finally, through the appropriate Jacobian transformation we have presented data directly comparable to that obtained in restricted geometry experiments and find cross sections $d^2\sigma/d\Omega_1 d\Omega_2$ very close to the Harvard 158-MeV coplanar measurements at $\theta=30°$ and 35°. Theoretical calculations for the restricted geometry done by Duck and Pearce and by Sobel and Cromer generally agree with the data taken thus far in the energy range 33.5 to 204 MeV.